Journal of Materials Chemistry A

Accepted Manuscript

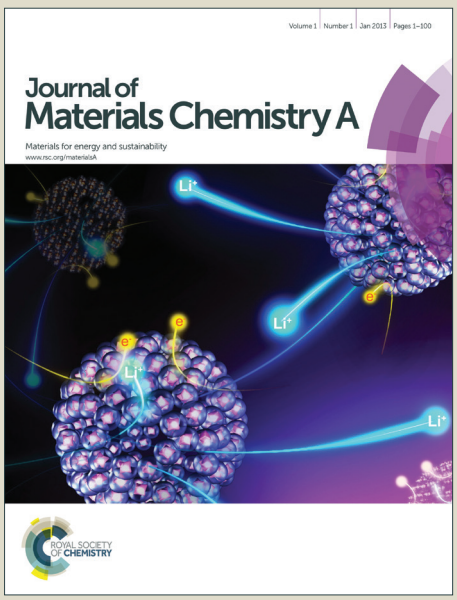

ROYAL SOCIETY OF CHEMISTRY

www.rsc.org/materialsA

ARTICLE TYPE www.rsc.org/xxxxxx | XXXXXXXX

Multiphase Sodium Titanate/Titania Composite Nanostructures as Pt-based Catalyst Supports for Methanol Oxidation

Xu-Lei Sui [1,2], Zhen-Bo Wang [1,], Cun-Zhi Li[1,2], Jing-Jia Zhang [1], Lei Zhao [1], Da-Ming Gu [2*], Shuo Gu[3]*

Received (in XXX, XXX) Xth XXXXXXXXX 201X, Accepted Xth XXXXXXXXX 201X

First published on the web Xth XXXXXXXXX 201X
DOI: 10.1039/b000000x

Sodium titanate/titania composite nanotubes/nanorods (STNS) are synthesized from anatase titania by hydrothermal method and subsequent annealing in the range of 300-700 °C. The changes of STNS in composition and morphology are investigated by X-ray diffraction (XRD) and transmission electron microscopy (TEM). The results reveal that the composition of STNS changes from "$Na_{2-x}H_xTi_2O_5$" to "$Na_2Ti_6O_{13}$" and its morphology changes from nanotube to nanorod. The products of 400 °C and 600 °C correspond to the intermediate state of reactions. Pt-based catalysts are prepared by microwave-assisted ethylene glycol process, and are also characterized by physical analysis and electrochemical measurement. The variations of catalytic activity and stability of Pt/C-STNS catalysts show the interesting "M" shape with the increasing of annealing temperature of STNS. The Pt nanoparticles supported on STNS-400 nanotubes and STNS-600 nanorods exhibit more uniform dispersion and superior electrocatalystic performance for methanol electrooxidation. The main reason seems to be that both of them are multiphase composites with a large number of phase interfaces and crystal defects, which is conducive to the deposition of Pt nanoparticles. The uniform dispersion of Pt nanoparticles plays an essential role in the electrochemical performance of catalysts. In addition, the presence of "anatase TiO_2" phase in both of them can further enhance the electrochemical performance due to the metal-support interaction. Moreover, compared to commercial Pt/C, the Pt/C-STNS-600 catalyst exhibits higher electrochemical activity and stability, suggesting that superior catalyst can be developed by designing the structure and composition of the supports.

1. Introduction

The direct methanol fuel cell (DMFC) is considered to be a promising power source for portable electronic devices and electric vehicles in view of its lower weight and volume[1, 2]. Although DMFC has been greatly developed in recent decades, some obstacles, such as the expensive cost of catalyst, the poisoning of intermediates, methanol crossover and methanol toxicity, still exist and impede its wide commercialization[3, 4]. A large number of researchers pay particular attention to minimize the platinum loading and keep the high catalytic activities and durability of Pt-based catalysts with better tolerance against the CO_{ads} poisoning. The widely accepted methods are to disperse Pt nanoparticles on large surface area supports[5, 6] and develop Pt-based alloys[7-9] or Pt/metal oxide composite[10] catalysts based on the bifunctional mechanism and electronic effect.

Usually, carbon-based material is the most commonly used catalyst support[11]. Carbon powder as catalyst support has been commercialized. However, carbon corrosion leads to the decrease of catalytic activity during the long term operation of DMFC[12]. To improve the stability of carbon powder, graphitized carbon materials are developed, such as carbon nanotubes[13-16] and graphene[17, 18]. In previous studies, graphene has attracted particular attention due to its large surface area, high conductivity and good stability[19]. However, graphitized carbon materials are not conducive to the deposition of Pt nanoparticles[20]. In addition, the problem of CO_{ads} poisoning has not yet been solved.

Metal oxide as catalyst support is always a hot research topic. Various possible metal oxide supports have been studied, such as SnO_2 [21, 22], TiO_2 [23, 24], CeO_2 [25, 26], Nb_2O_5 [27]. Among them, titania is of particular interest due to its low cost and inherent stability in electrochemical environment, as well as the strong metal-support interactions[24, 28]. Therefore, to explore the possibility of employing titania as catalyst support in methanol electrooxidation is very necessary and meaningful. But its low electron conductivity greatly reduces catalytic performance of Pt-based catalysts. Therefore, it necessarily deserves the investigation of special structural design to improve its electron conductivity. Titania nanotubes[29-31] and hydrogenotitanate nanotubes[32] have been proved to be an effective strategy.

In this work, we successfully synthesized sodium titanate /titania composite nanotubes/nanorods (STNS) by the typical hydrothermal method and subsequent annealing at the different temperatures. The composition and morphology of STNS were closely related to the annealing temperature, and the changing process was deeply and systematically analyzed. The Pt

[a] *School of Chemical Engineering and Technology, Harbin Institute of Technology, No.92 West-Da Zhi Street, Harbin, 150001 China. E-mail: wangzhb@hit.edu.cn; Tel.: +86-451-86417853; Fax: +86-451-86418616*
[b] *School of Science, Harbin Institute of Technology, No.92 West-Da Zhi Street, Harbin, 150001 China*
[c] *Department of Electrical and Computer Engineering, The George Washington University, Washington, DC, 20052, USA*

† Electronic supplementary information (ESI) available. See DOI: 10.1039/b000000x

nanoparticles were deposited on the mixture support of carbon and STNS through a microwave-assisted polyol process. The effects of annealing temperature on the catalytic performance of Pt catalysts were investigated in details.

2. Experimental

2.1. Materials preparation

2.1.1 Synthesis of sodium titanate/titania composite nanostructures. Sodium titanate/titania composite nanostructures (STNS) were prepared by hydrothermal method[33]. The preparation process was described as follows: (1) 500 mg TiO_2 power was dispersed in 150 mL NaOH aqueous solution (10 mol·L^{-1}) and placed in a Teflon-lined stainless-steel autoclave. (2) The autoclave was heated at 130 °C for 24 h in the constantly rotating condition. (3) The dispersion was allowed to cool and washed with deionized water for several times. (4) The pH value of dispersion was adjusted with dilute HNO_3 to about 7.0 and kept being immersed for 4 h. (5) The samples were filtered and dried at 80 °C for 5 h, followed by calcination at 300 °C, 400 °C, 500 °C, 600 °C, and 700 °C, respectively, under air for 2 h (STNS-300, 400, 500, 600, and 700).

2.1.2 Preparation of Pt/C-STNS catalysts. Pt nanoparticles were respectively deposited on the mixture of carbon black and STNS by a microwave-assisted ethylene glycol process to synthesize Pt/C-STNS catalyst. In order to produce 20 wt% Pt loading catalysts, 25 mg STNS and 25 mg Vulcan XC-72 carbon black were dispersed into the 60 mL mixed solution of ethylene glycol (EG) and isopropyl alcohol (V/V=4:1) under ultrasonic treatment for 1 h, and then adding an appropriate amount of H_2PtCl_6-EG solution with a subsequent stirring process for 3 h. The mixture was adjusted to pH 12.0 with NaOH-EG solution. After being saturated with argon, the suspension was heated by microwave for 55 s. While the suspension was cooled to room temperature, the pH value was adjusted to 2.0～3.0 by HNO_3 for 12 h to precipitate platinum nanoparticles. Finally, the catalysts were filtered and washed with a large amount of deionized water and dried under vacuum at 80 °C for 5 h.

2.2 Characterizations of physical properties

The crystal structure of the samples was characterized by X-ray diffraction (XRD) analysis using a D/max-RB diffractometer (made in Japan) with a Cu Ka X-ray source, scanning between 5° and 90° at a rate of 4° min^{-1}. Transmission electron microscopy (TEM, Japan JEOLJEM-2010EX) was used for the morphology of the samples. X-ray energy-dispersive spectra (EDAX) were acquired using a Hitachi-S-4700 analyzer connected with a scanning electron microscope (SEM, Hitachi Ltd. S-4700).

2.3 Electrochemical measurements

All the electrochemical measurements were carried out at 25 °C in a typical three electrodes cell using a CHI 650E electrochemical analysis instrument. A platinum network and Hg/Hg_2SO_4 electrode (MSE, 0.64 V relative to normal hydrogen electrode, NHE) were used as the counter and reference electrodes, respectively. The solution of 0.5 mol·L^{-1} H_2SO_4 was used as the supporting electrolyte. In addition, the solution of 0.5 mol·L^{-1} H_2SO_4 containing 0.5 mol·L^{-1} CH_3OH was used for the oxidation activity test. Before the electrochemical measurements, argon was bubbled in the electrolyte for 20 min.

The working electrode was prepared as follows. 2.0 mg catalyst in 1.0 mL ultrapure water was ultrasonicated for 20 min to form the catalyst ink. Then, 5 μL catalyst ink and 5 μL dilute aqueous Nafion® solution were successively dropped on a glassy carbon with 4 mm diameter.

The cyclic voltammograms (CV) were carried out at 50 mV·s^{-1} from -0.64 to 0.51 V (*vs.* MSE), and the onset potential was obtained at the scan rate of 0.5 mV·s^{-1}. The working electrodes were completely activated before the measurement curves were recorded. The electrochemical active surface areas (ESA) of platinum were calculated with the formula $ESA_{pt}=Q_H/(0.21\cdot M_{Pt})$[34]. Q_H is the charge due to the hydrogen adsorption/desorption in the hydrogen region of the CVs. Electrochemical impendence spectroscopy (EIS) were obtained at frequencies between 100 kHz and 0.01 Hz with 12 points per decade. The amplitude of the sinusoidal potential signal was 5 mV. The amperometric *i–t* curves were obtained at a constant potential of 0.6 V for 3600 s in methanol acidic medium.

3. Results and discussion

3.1. Physical characterization of various supports and catalysts

The formation process of STNS has been detailed described in our previous work. After the course of washing and acid treatment, the obtained product is $Na_{2-x}H_xTi_2O_5\cdot H_2O$ nanotube. According to our latest research, it can be found that the annealing temperature is a key factor to the composition and morphology of STNS.

The phase component changes of STNS products are investigated by XRD at different annealing temperatures. Fig. 1 shows the XRD patterns of STNS products prepared at different annealing temperatures. (1) In the XRD pattern of STNS-300, the broad reflection peaks are observed at 2θ = 9.2°, 24.3°, 28.1°and 48.1°, which reveal the presence of "$Na_{2-x}H_xTi_2O_5$" phase. (2) In the XRD pattern of STNS-400, the intensity of broad reflection peaks decreases compared to that of STNS-300 which indicates

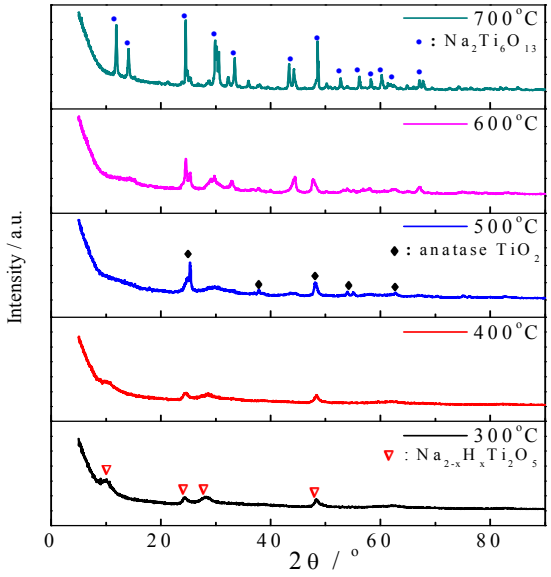

Fig. 1 XRD patterns of STNS products prepared at different annealing temperatures

that part of "$H_2Ti_2O_5$" phase is converted to "TiO_2" phase. (3) In the XRD pattern of STNS-500, the reflection peaks of 23.3°, 37.8°, 48.1°, 54.0° and 62.8° reveal the presence of "anatase TiO_2" phase. At the same time, the reflection peaks of "$Na_2Ti_2O_5$" phase are still present, but their intensities significantly decrease, which may be because all of "$H_2Ti_2O_5$" phase is converted to "TiO_2" phase and only "$Na_2Ti_2O_5$" phase remains. (4) In the XRD pattern of STNS-600, new reflection peaks appear compared to those of STNS-500, which indicate the formation of new phase. (5) In the XRD pattern of STNS-700, the reflection peaks are exactly consistent with the standard reflection peaks of "$Na_2Ti_6O_{13}$" phase (JCPDS card: 73-1398). These results demonstrate that the composition of STNS products is continuously changing with the annealing temperature from 300 °C to 700 °C. The products of 300 °C, 500 °C and 700 °C correspond to the final state of reaction while the products of 400 °C and 600 °C correspond to the intermediate state of reaction. The reaction formulas can be written as follows (Eqn.(1) and Eqn.(2)) :

$$H_2Ti_2O_5 \cdot H_2O \rightarrow TiO_2 + H_2O \quad (1)$$

$$Na_2Ti_2O_5 + TiO_2 \rightarrow Na_2Ti_6O_{13} \quad (2)$$

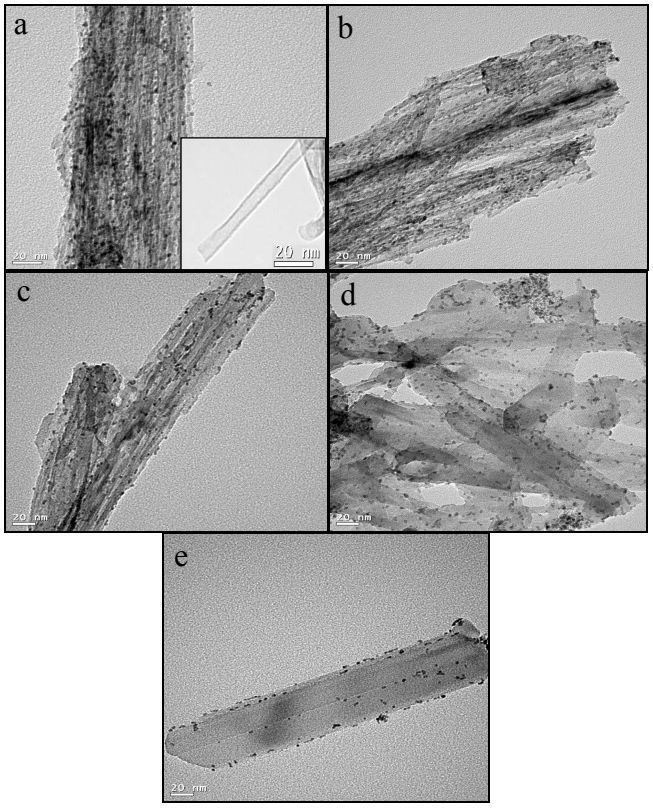

Fig. 2 TEM images of Pt/C-STNS catalysts (a: 300 °C; b: 400 °C; c: 500 °C; d: 600 °C; e: 700 °C); the inset is the image of STNS-300

TEM images of catalysts Pt/C-STNS-300 (a), 400 (b), 500 (c), 600 (d) and 700 (e) are shown in Fig. 2. It is clearly seen that the morphology of STNS products changes from nanotube to nanorod with the increasing of annealing temperature. The morphology of nanotube can be evidently seen in the inserted picture of Fig. 2a, while the morphology of nanorod can be seen in Fig. 2e. The diameters of STNS change from about 10 nm to 40 nm. When the annealing temperature is low, the morphology remains to be nanotube. The diameter of STNS nanotubes is small to be less than 10 nm. Therefore, STNS nanotubes are easy to reunite as shown in Fig. 2. As the increasing of annealing temperature, the agglomerated nanotubes react with each other resulting in the changes of STNS products in morphology and size. In addition, carbon is present in all catalysts, but the role of STNS on the morphology and performance is mainly concerned. Therefore, TEM images only show the region of STNS.

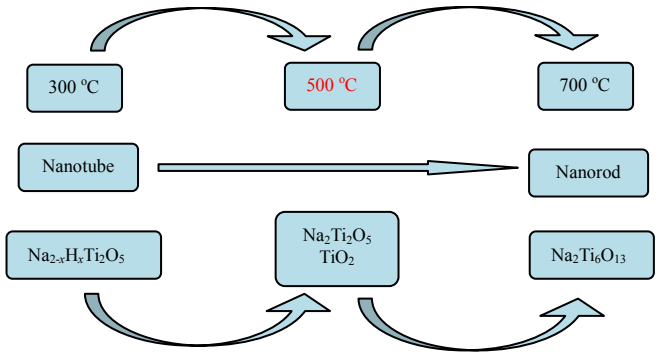

Scheme 1 Schematic diagram of the change process of STNS

Through the above XRD and TEM analysis, the composition and morphology of different STNS products are determined. The change process is shown in Scheme 1. The product obtained at the annealing temperature of 300 °C is $Na_{2-x}H_xTi_2O_5$ ($Na_2Ti_2O_5$ and $H_2Ti_2O_5$) nanotube. After the temperature raise to 500 °C, $H_2Ti_2O_5$ is completely converted to TiO_2. As the temperature continues to rise to 700 °C, $Na_2Ti_6O_{13}$ nanorod is obtained by the reaction of $Na_2Ti_2O_5$ and TiO_2. In addition, the change from nanotube to nanorod occurs in the whole course of reaction. When the annealing temperatures are 400 °C and 600 °C, the products obtained are multiphase composites, respectively, "$Na_2Ti_2O_5$, $H_2Ti_2O_5$, TiO_2" and "$Na_2Ti_2O_5$, TiO_2, $Na_2Ti_6O_{13}$". The multiphase composites have many phase interfaces and crystal defects,

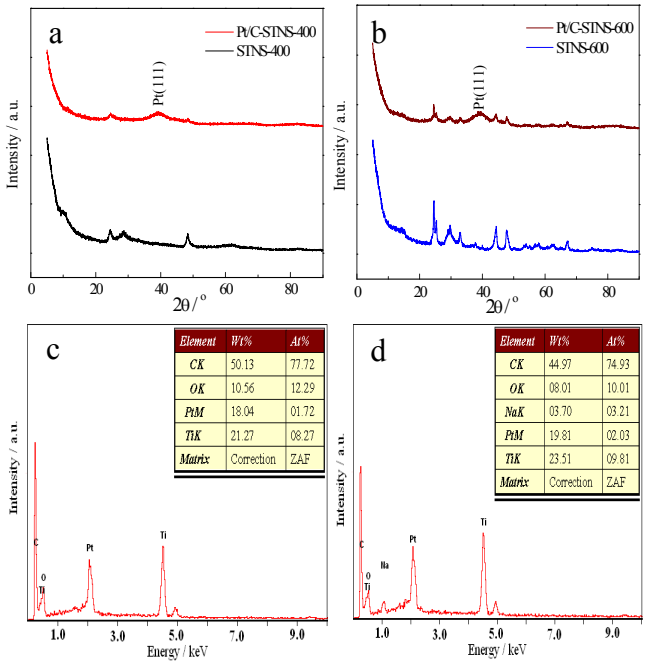

Fig. 3 XRD and EDX patterns of Pt/C-STNS-400 (a, c) and Pt/C-STNS-600 (b, d)

conducive to the deposition of Pt nanoparticles. The XRD patterns of Pt/C-STNS-400 (a) and Pt/C-STNS-600 (b) are shown in Fig. 3. The representative diffraction peaks of Pt (111) are shown in spectra (a, b). Because the face-centered cubic (f.c.c.) phase is the only structure for platinum, the Pt metal is subsistent in the form of a face-centered cubic (f.c.c.) phase. The influence of STNS peaks makes Pt peaks concealed partly, however, the peak of Pt(111) is distinctly observed. Besides, the Pt mass contents of Pt/C-STNS-400 (c) and Pt/C-STNS-600 (d) catalysts are determined by EDX analysis as shown in Fig. 3, respectively, 18.04 wt.% and 19.81 wt.%. Because the production processes are the same and the yields of all catalysts are very close, It can be confirmed that the Pt loadings of all catalysts are similar to the theoretical value of 20 wt.%. In addition, the disappearance of sodium element in Pt/C-STNS-400 catalyst is maybe because $Na_2Ti_2O_5$ is converted to $H_2Ti_2O_5$ during the synthesis of catalyst. The distribution of platinum nanoparticles on STNS products can be seen from Fig. 2. By comparison, it can be found that the distribution of Pt nanoparticles on STNS-400 nanotubes and STNS-600 nanorods are more uniform than others. It is maybe because STNS-400 nanotubes and STNS-600 nanorods are multiphase composites with a large number of phase interfaces and crystal defects. This configuration facilitates the uniform deposition of Pt nanoparticles.

3.2 Electrochemical performance of various catalysts

Fig. 4a shows cyclic voltammograms of Pt/C-STNS catalysts obtained at 300 °C, 400 °C, 500 °C, 600 °C and 700 °C in acid medium (0.5 mol·L^{-1} H_2SO_4). It can be seen that all curves have three typical regions described as the hydrogen region, the double layer region and the oxygen region. The electrochemical active specific surface areas (ESA_{Pt}) of Pt/C-STNS catalysts are obtainedby measurements of the hydrogen adsorption–desorption (HAD) integrals. The variation of ESA_{Pt} can be clearly seen with different annealing temperatures in Fig. 4b. The ESA_{Pt} of Pt/C-STNS catalysts are 49.8, 60.5, 54.3, 63.7 and 56.2 $m^2 \cdot g^{-1}$ at the annealing temperatures of 300 °C, 400 °C, 500 °C, 600 °C and 700 °C, respectively. There are two peaks at the annealing temperature of 400 °C and 600 °C. The variation of "M" shape is not conventional and very interesting. Combining the physical characterization above, we find that the ESA_{Pt} variation of Pt/C-STNS catalysts is closely related to the composition of STNS products. The products of STNS-400 and STNS-600 correspond to the intermediate state of reaction. A large number of phase interfaces and crystal defects make the deposition of Pt nanoparticles more uniform in favor of catalytic reaction. Meanwhile, the presence of "anatase TiO_2" phase can enhance the strong metal-support interaction (SMSI)[23, 35]. In addition, the Pt/C-STNS-600 catalyst exhibits the highest ESA, demonstrating that the catalyst has the best electrochemical activity.

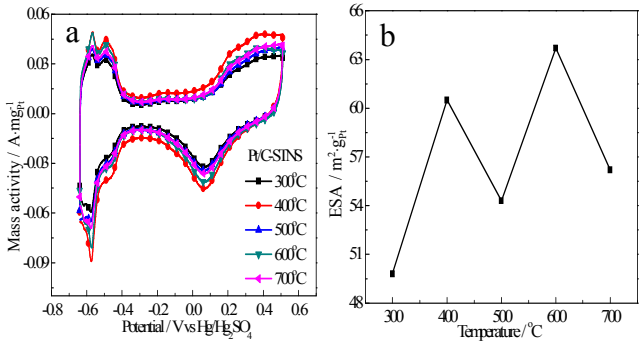

Fig. 4 Cyclic voltammograms of catalysts in 0.5 mol L^{-1} H_2SO_4 (a) and relationship of ESA_{Pt} of catalysts and annealing temperatures (b)

The cyclic voltammograms of Pt/C-STNS catalysts at different annealing temperatures are obtained in methanol acidic medium (0.5 mol·L^{-1} H_2SO_4 + 0.5 mol·L^{-1} CH_3OH). In order to facilitate observation, the CV curves of Pt/C-STNS-300, 400 and 500 are shown in Fig. 5a, and the CV curves of Pt/C-STNS-500, 600 and 700 are shown in Fig. 5b. For the anodic oxidation of methanol, the forward peak mass current density is generally regarded as methanol oxidation on non-poisoned catalysts. Therefore, the forward peak mass current density can reflect the electrochemical activity of catalysts. Therefore, the variations of the forward peak current density are exhibited in Fig. 5c. The forward peak mass current density are 0.38, 0.46, 0.41, 0.48 and 0.44 A·mg$^{-1}_{Pt}$ at the annealing temperature of 300 °C, 400 °C, 500 °C, 600 °C and 700 °C, respectively. The variation of "M" shape appears again, indicating that the regularity is not accidental. Furthermore, the onset potential, which is the activation energy needed in order for catalysts to trigger the methanol oxidation, is an important parameter that reflects the catalytic activity of a catalyst. A low onset potential reveals a high efficiency of a catalytic reaction. As indicated by dashed lined in Fig. 5d, the onset potential is found to be in the order: Pt/C-STNS-600 < Pt/C-STNS-400 < Pt/C-STNS-700 < Pt/C-STNS-500 < Pt/C-STNS-300, exhibiting the same regularity of "M" shape. The results further indicate that the composition of STNS plays an important role on the performance of Pt/C-STNS catalysts.

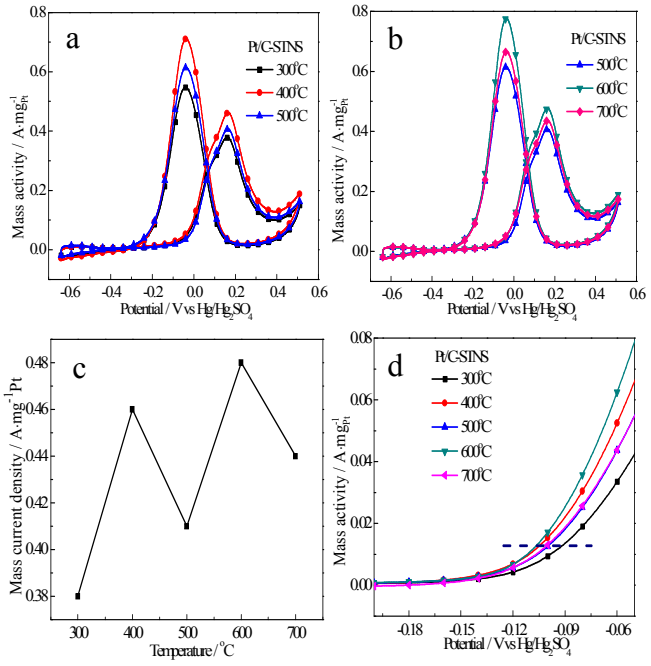

Fig. 5 Cyclic voltammograms of catalysts in methanol acidic medium at the scan rate of 50 mV·s^{-1} (a,b); relationship of peak mass current density and annealing temperatures (c); linear sweep voltammetry at the scan rate of 0.5 mV·s^{-1}(d)

Electrochemical impendence spectroscopy (EIS) can be used as an effective method for measuring the charge transfer resistance, which reflects the activity of catalyst for methanol electrooxidation. The nyquist plot of Pt/C-STNS catalysts for methanol electrooxidation is shown in Fig. 6. The size of the semicircle directly reflects the strength of the electrochemical reaction resistance. It can be seen from Fig. 6 that the same regularity appears and the semicircles of Pt/C-STNS-400 and 600 catalysts are smaller than other catalysts, indicating that their methanol electrooxidation rates are much faster than other catalysts. In order to easily observe the impedance behavior, the resistances can be obtained from the analysis of EIS spectra by using the software of Z-view based on an equivalent electric circuit[36] and the simulated results are shown in Table 1. The chargetransfer resistances (R_{ct}) of Pt/C-STNS-300, 400, 500, 600 and 700 catalysts are 88.7, 73.7, 93.9, 71.9 and 86.8 $\Omega\cdot cm^2$, respectively. The variation of chargetransfer resistance is consistent with that of cyclic voltammograms test above.

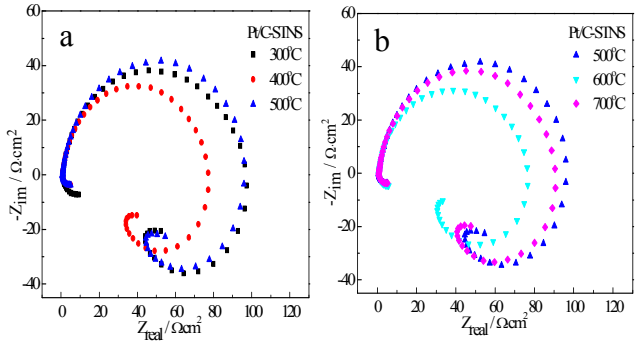

Fig. 6 Nyquist plot of catalysts in methanol acidic medium (a, b)

Table 1 The simulated results of impedance behaviour

Annealing temperature(°C)	300	400	500	600	700
$R_{ct}(\Omega\cdot cm^2)$	88.7	73.7	93.9	71.9	86.8
$R_u(\Omega\cdot cm^2)$	0.98	0.86	0.80	0.83	0.87

The amperometric *i–t* curves of Pt/C-STNS catalysts are obtained at a constant potential of 0.6 V for 3600 s in methanol acidic medium (0.5 $mol\cdot L^{-1}$ H_2SO_4 +0.5 $mol\cdot L^{-1}$ CH_3OH). As shown in Fig. 7, Pt/C-STNS-600 catalyst has the highest mass current density during 3600 s. The final current densities after 3600s are 0.013, 0.024, 0.016, 0.035 and 0.019 $A\cdot mg^{-1}$ at the annealing temperatures of 300 °C, 400 °C, 500 °C, 600 °C and 700 °C, respectively. The stability of Pt/C-STNS catalysts can be obtained by calculating the ratio of the final current to the maximum current. The retention rates of mass current density are 13.7%, 23.3%, 18.0%, 26.3% and 19.0% at the annealing temperature of 300 °C, 400 °C, 500 °C, 600 °C and 700 °C, respectively. The variations of the activity and stability both show the interesting "M" shape, as is consistent with the cyclic voltammograms (CVs) and electrochemical impedance spectroscopy (EIS).

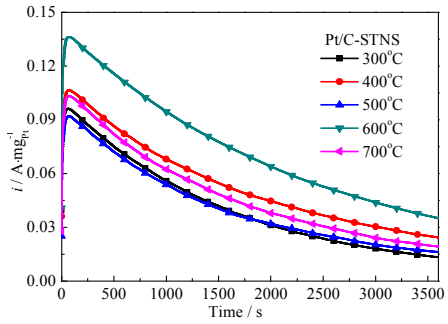

Fig. 7 Amperometric *i–t* curves of catalysts in methanol acidic medium

At present, Pt/C is the only commercial catalyst because of its excellent electrocatalytic performance. Therefore, the commercial 20 wt. % Pt/C catalyst (Johnson Matthey Corp.) is used as a reference to evaluate the electrocatalytic performance of the catalyst supported on STNS nanostructure as shown in Fig. 8. The electrochemical active specific surface area (ESA) is determined through the charge of hydrogen adsorption/desorption in 0.5 $mol\cdot L^{-1}$ H_2SO_4 solution from Fig. 8a. The ESA is 63.7 $m^2\cdot g^{-1}$ for Pt/C-STNS-600 and 54.1 $m^2\cdot g^{-1}$ for Pt/C. The difference of their ESA is 9.6 $m^2\cdot g^{-1}$ and much larger than the error range of ±5%, demonstrating that the activity of Pt/C-STNS-600 catalyst is higher than Pt/C. For methanol oxidation as shown in Fig. 8b, the forward peak current densities on Pt/C-STNS-600 and Pt/C are about 0.48 and 0.36 $A\cdot mg^{-1}_{Pt}$, respectively. The activity of Pt/C-STNS-600 catalyst is 1.3 times higher than that of Pt/C. In addition, as shown

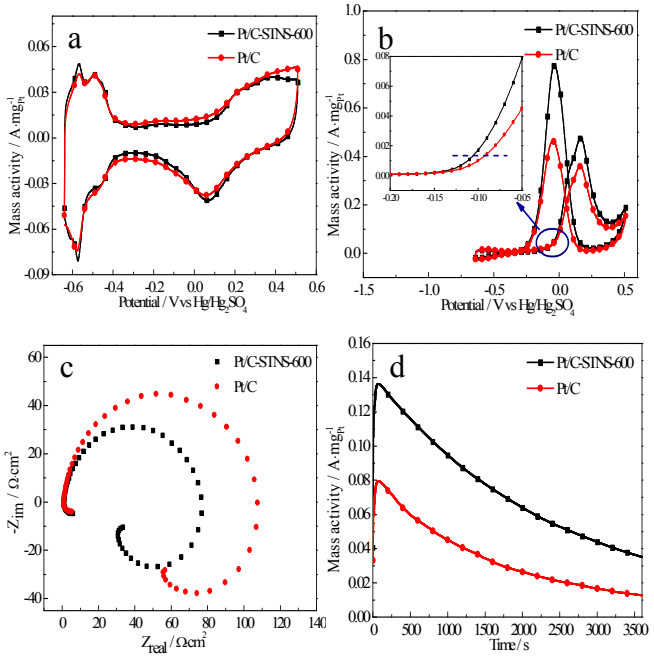

Fig. 8 Electrochemical performance of Pt/-STNS-600 and Pt/C catalysts: cyclic voltammograms at the scan rate of 50 $mV\cdot s^{-1}$ in 0.5 $mol\cdot L^{-1}$ H_2SO_4 (a) and in methanol acidic medium (b), the inset is the linear sweep voltammetry at the scan rate of 0.5 $mV\cdot s^{-1}$; Nyquist plot in methanol acidic medium (c); amperometric *i–t* curves in methanol acidic medium (d)

in the inset of Fig. 8b, the onset potential of Pt/C-STNS-600 is lower than that of Pt/C because of the synergistic effect between Pt and STNS, further indicating that the activity of Pt/C-STNS-600 is higher. The result is consistent with the electrochemical impendence spectroscopy as shown in Fig. 8c. The smaller semicircle of Pt/C-STNS-600 catalyst compared to that of Pt/C catalyst stands for much faster rate of methanol oxidation. The amperometric *i–t* curves can simultaneously reflect the activity and stability of catalysts. It can be seen from Fig. 8d that the final mass current density of Pt/C-STNS-600 after 3600s is 0.035 $A \cdot mg^{-1}$, higher than 0.013 $A \cdot mg^{-1}$ of Pt/C. At the same time, the retention rates of mass current density for Pt/C-STNS-600 and Pt/C catalysts are about 26.3% and 16.3%, respectively. Overall, the Pt/C-STNS-600 catalyst shows better electrochemical activity and stability, compared with those of the commercial Pt/C catalyst. The improvements of activity and stability for Pt/C-STNS-600 catalyst can be ascribed to the synergetic effect between Pt and TiO_2, which can enhance the electrocatalytic performance effectively [23, 35].

4. Conclusions

In this study, sodium titanate/titania composite nanotubes/nanorods were by hydrothermal method and subsequent annealing in the range of 300-700 ^oC. The annealing temperature is proved to play an essential role in changing the composition of "$Na_{2-x}H_xTi_2O_5$" to "$Na_2Ti_6O_{13}$" and the morphology of nanotube to nanorod. Pt-based catalysts were synthesized by microwave-assisted ethylene glycol process. The Pt nanoparticles supported on the products obtained at the annealing temperature of 400 ^oC and 600 ^oC show better dispersion, resulting in higher electrocatalytic performance than others. Moreover, the Pt/C-STNS-600 catalyst exhibits the better electrochemical activity and stability compared with the commercial Pt/C catalyst. The multiphase structure of supports should be the main reason of the improvements. A large number of phase interfaces and crystal defects generated from the multiphase structure result in the dispersion of Pt nanoparticles more uniform, which improves the electrocatalytic performance of Pt/C-STNS catalysts. In addition, the presence of "anatase TiO_2" phase in both of them can further enhance the electrochemical performance due to the metal-support interaction.

Acknowledgment

This research is financially supported by the National Natural Science Foundation of China (Grant No. 21273058), China postdoctoral science foundation (Grant No.2012M520731 and 2014T70350), Heilongjiang postdoctoral foundation (LBH-Z12089) and outstanding subject leaders of special fund project of Harbin in China (Grant No.2012RFXXG99).

References

1. A. Schroder, K. Wippermann, J. Mergel, W. Lehnert, D. Stolten, T. Sanders, T. Baumhofer, D. U. Sauer, I. Manke, N. Kardjilov, A. Hilger, J. Schloesser, J. Banhart and C. Hartnig, *Electrochem Commun*, 2009, **11**, 1606-1609.
2. A. Lam, D. P. Wilkinson and J. J. Zhang, *J Power Sources*, 2009, **194**, 991-996.
3. S. Yilmazturk, H. Deligoz, M. Yilmazoglu, H. Damyan, F. Oksuzomer, S. N. Koc, A. Durmus and M. A. Gurkaynak, *J Power Sources*, 2010, **195**, 703-709.
4. X. L. Li and A. Faghri, *J Power Sources*, 2013, **226**, 223-240.
5. V. Selvaraj and M. Alagar, *Electrochem Commun*, 2007, **9**, 1145-1153.
6. C. P. Liu, X. Z. Xue, T. H. Lu and W. Xing, *J Power Sources*, 2006, **161**, 68-73.
7. W. H. Zhong, Y. X. Liu and D. J. Zhang, *J Phys Chem C*, 2012, **116**, 2994-3000.
8. V. R. Stamenkovic, B. Fowler, B. S. Mun, G. F. Wang, P. N. Ross, C. A. Lucas and N. M. Markovic, *Science*, 2007, **315**, 493-497.
9. R. Ahmadi, M. K. Amini and J. C. Bennett, *J Catal*, 2012, **292**, 81-89.
10. K. S. Lee, I. S. Park, Y. H. Cho, D. S. Jung, N. Jung, H. Y. Park and Y. E. Sung, *J Catal*, 2008, **258**, 143-152.
11. J. Zhang, S. H. Tang, L. Y. Liao, W. F. Yu, J. S. Li, F. Seland and G. M. Haarberg, *J Power Sources*, 2014, **267**, 706-713.
12. J. J. Wang, G. P. Yin, Y. Y. Shao, S. Zhang, Z. B. Wang and Y. Z. Gao, *J Power Sources*, 2007, **171**, 331-339.
13. X. Wang, W. Z. Li, Z. W. Chen, M. Waje and Y. S. Yan, *J Power Sources*, 2006, **158**, 154-159.
14. Y. Y. Mu, H. P. Liang, J. S. Hu, L. Jiang and L. J. Wan, *J Phys Chem B*, 2005, **109**, 22212-22216.
15. L. Zhao, Z. B. Wang, X. L. Sui and G. P. Yin, *J Power Sources*, 2014, **245**, 637-643.
16. A. C. Johansson, J. V. Larsen, M. A. Verheijen, K. B. Haugshoj, H. F. Clausen, W. M. M. Kessels, L. H. Christensen and E. V. Thomsen, *J Catal*, 2014, **311**, 481-486.
17. M. Chen, Y. Meng, J. Zhou and G. W. Diao, *J Power Sources*, 2014, **265**, 110-117.
18. Y. J. Hu, P. Wu, Y. J. Yin, H. Zhang and C. X. Cai, *Appl Catal B-environ*, 2012, **111**, 208-217.
19. S. H. Hsieh, M. C. Hsu, W. L. Liu and W. J. Chen, *Appl Surf Sci*, 2013, **277**, 223-230.
20. J. B. Zhu, X. Zhao, M. L. Xiao, L. Liang, C. P. Liu, J. H. Liao and W. Xing, *Carbon*, 2014, **72**, 114-124.
21. J. W. Magee, W. P. Zhou and M. G. White, *Appl Catal B-environ*, 2014, **152**, 397-402.
22. E. Higuchi, T. Takase, M. Chiku and H. Inoue, *J Power Sources*, 2014, **263**, 280-287.
23. Z. Z. Jiang, Z. B. Wang, Y. Y. Chu, D. M. Gu and G. P. Yin, *Energy & Environmental Science*, 2011, **4**, 728-735.
24. Q. Lv, M. Yin, X. Zhao, C. Y. Li, C. P. Liu and W. Xing, *J Power Sources*, 2012, **218**, 93-99.
25. Y.-Y. Chu, Z.-B. Wang, Z.-Z. Jiang, D.-M. Gu and G.-P. Yin, *Adv Mater*, 2011, **23**, 3100-3104.
26. H. L. Chen, J. L. Duan, X. L. Zhang, Y. F. Zhang, C. Guo, L. Nie and X. W. Liu, *Mater Lett*, 2014, **126**, 9-12.
27. P. Justin, P. H. K. Charan and G. R. Rao, *Appl Catal B-environ*, 2010, **100**, 510-515.
28. S. Y. Huang, P. Ganesan, S. Park and B. N. Popov, *J Am Chem Soc*, 2009, **131**, 13898-13899.
29. C. K. Zhang, H. M. Yu, Y. K. Li, W. Song, B. L. Yi and Z. G. Shao, *Electrochim Acta*, 2012, **80**, 1-6.
30. H. Y. Li, J. S. Wang, M. Liu, H. Wang, P. L. Su, J. S. Wu and J. Li, *Nano Research*, 2014, **7**, 1007-1017.
31. Y. Q. Liang, Z. D. Cui, S. L. Zhu, Y. Liu and X. J. Yang, *J Catal*,

2011, **278**, 276-287.
32. B. Abida, L. Chirchi, S. Baranton, T. W. Napporn, C. Morais, J. M. Leger and A. Ghorbel, *J Power Sources*, 2013, **241**, 429-439.
33. T. Kasuga, M. Hiramatsu, A. Hoson, T. Sekino and K. Niihara, *Adv Mater*, 1999, **11**, 1307-1311.
34. X. S. Peng, K. Koczkur, S. Nigro and A. C. Chen, *Chem Commun*, 2004, 2872-2873.
35. Z. Z. Jiang, Z. B. Wang, Y. Y. Chu, D. M. Gu and G. P. Yin, *Energy & Environmental Science*, 2011, **4**, 2558-2566.
36. Y. H. Lin, X. L. Cui, C. H. Yen, C.M. Wai, *Langmuir*, 2005, 21, 11474-11479.

Multiphase sodium titanate/titania Composite Nanostructures as Pt-based Catalyst supports for Methanol Oxidation

Xu-Lei Sui, Zhen-Bo Wang, Cun-Zhi Li, Jing-Jia Zhang, Lei Zhao,Da-Ming Gu *, Shuo Gu*

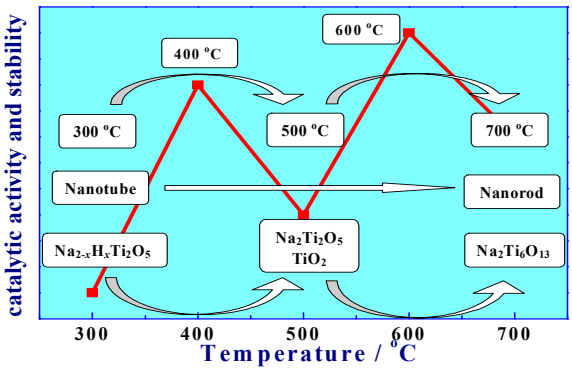

The performance variations of catalysts show the "M" shape, which is closely related to the phase change of supports.